

Characterization of Zn-Doped MgTiO₃ Powders Synthesized by Dissolved Metals Mixing Method

Musyarofah Musyarofah^{1*}, Isao Tanaka², Zakiah Mohamed³, Yingyot Poo-arporn⁴, Lusi Ernawati⁵, Gatut Yudoyono⁶, and Budi Prayitno⁷

¹Department of Physics, Institut Teknologi Kalimantan, Jl. Soekarno-Hatta Km. 15, Balikpapan 76127, Indonesia

²Department of Materials Science and Engineering, Kyoto University, Sakyo, Kyoto 606-8501, Japan

³Faculty of Applied Sciences, Universiti Teknologi MARA, Shah Alam, Selangor 40450, Malaysia

⁴Synchrotron Light Research Institute (SLRI), Nakhon Ratchasima 30000, Thailand

⁵Department of Chemical Engineering, Institut Teknologi Kalimantan, Jl. Soekarno-Hatta Km. 15, Balikpapan 76127, Indonesia

⁶Department of Physics, Institut Teknologi Sepuluh Nopember, Jl. Arief Rahman Hakim, Surabaya 60111, Indonesia

⁷Department of Mechanical Engineering, Universitas Balikpapan, Jl. Pupuk Raya, Balikpapan 76114, Indonesia

* **Corresponding author:**

email: musyarofah@lecturer.itk.ac.id

Received: May 5, 2024

Accepted: December 11, 2024

DOI: 10.22146/ijc.95879

Abstract: Zn-doped magnesium titanate powders with different Zn compositions, $x = 0$ to 1, were synthesized using the dissolved metals mixing method. The roles of calcination temperature and dopant Zn composition on powder morphology, phase composition, crystallite size, crystalline cell volume, and local environment were investigated through scanning electron microscope (SEM) observation, Rietveld analysis of powder X-ray diffraction (XRD), Fourier transform infrared (FTIR) spectroscopy and X-ray absorption spectroscopy (XAS) for Ti K-edge X-ray absorption near edge structures (XANES). We found that the geikielite solid solutions were formed during the pre-calcination at 400 °C for 1 h. Results show spherical particles (~1 μm) with minimal size variation across calcination temperatures (600–800 °C) and Zn compositions, though some agglomeration occurs. After calcination at 600 °C for 4 h, the crystalline cell volume of geikielite was proportional to the Zn composition, implying the formation of the solid solution in the range of Zn composition up to the level close to $x = 1$. This successful synthesis of the Zn-doped magnesium titanate nanocrystals at temperatures much lower than those required by the solid-state reaction method was thereby well demonstrated.

Keywords: geikielite; dissolved metals mixing method; calcination; Zn-doped; structural properties

■ INTRODUCTION

Magnesium titanate (MgTiO₃) is a highly sought-after ceramic material due to its extensive use in several electronic components and devices, including capacitors, resonators, and microwave antennas. These applications are possible because of their unique properties. MgTiO₃ has a high dielectric constant due to its ability to store large amounts of electrical energy when exposed to an electric field, making it ideal for use in capacitors [1-2]. It also has a minimal dielectric loss for maintaining the

efficiency of electronic components [3]. The negligible coefficient in MgTiO₃'s resonant frequency remains stable under various circumstances, which is important for applications in resonators and antennas where precise frequency control is required [4]. MgTiO₃ is categorized as a semiconductor material with broad band-gap properties [5]. This property makes MgTiO₃ suitable for applications in photo-electrochemistry, where the material can interact with light to generate and control electron flow. In particular, it can be used in

anodes for dye sensitized solar cells (DSSCs). MgTiO_3 's unique properties make it a promising candidate as an alternative to titanium oxide in DSSCs [6]. DSSCs are a type of solar cell that uses a dye to absorb light and generate electrical current. MgTiO_3 's suitability for photo-electrochemical applications suggests it could offer advantages over traditional titanium oxide anodes in terms of efficiency and performance.

Exploring the connection between a material's structure and its physical attributes has been a focal point in research aimed at broadening its potential applications. Variations in structure stemming from differences in synthesis processes or the selection of raw materials can significantly influence material properties [7]. One such physical property that can be impacted by the material's structure is its ability to absorb electromagnetic waves. Some materials have a highly ordered atomic structure at the nanoscale, meaning that their atoms are arranged precisely and regularly in a manner at extremely small dimensions. Additionally, these materials may contain impurity atoms, also known as dopants, which are incorporated into their crystal lattice. These dopants can significantly impact the material's properties [8]. Materials with nanoscale order and dopants can exhibit unique interactions with electromagnetic waves, including visible light and other parts of the electromagnetic spectrum. These interactions can lead to interesting optical properties in the material.

Before we can fully understand and predict the optical characteristics of a material like MgTiO_3 , it's crucial to have a precise understanding of its crystal structure and the arrangement of atoms at the local level. In other words, we need to know how the atoms are organized within the material. X-ray absorption spectroscopy (XAS) is a well-established scientific technique used to study the composition, oxidation states of atoms, and local atomic structures in materials [9-10]. XAS is suggested as a powerful tool for investigating the local environment of a given element in the MgTiO_3 system. This information is essential for understanding how MgTiO_3 interacts with electromagnetic waves, which is crucial for studying its optical characteristics or any other property related to its structure. In this investigation, we conducted XAS research

on MgTiO_3 powders doped with zinc (Zn).

Several methods have been explored to synthesize titanate-based systems, each presenting unique benefits and limitations [11-12]. Common techniques include the sol-gel process, where a colloidal suspension transforms into a gel and subsequently solidifies; the dissolution process, which involves dissolving precursor materials in a solvent to create a homogeneous solution before further processing; coprecipitation, where multiple substances are simultaneously precipitated from a solution to form a solid; and solid-state reactions, which involve directly heating and reacting solid precursor powders to form the desired compound. However, achieving high purity and uniformity in the final product, especially through solid-state reactions, can be challenging due to incomplete mixing and high reaction temperatures.

An alternative approach reported in prior studies involves mixing dissolved metal components in an acidic solution to produce MgTiO_3 nanocrystals [13]. This method, known for yielding high-purity crystalline oxide materials, minimizes impurities by first dissolving metal components, which promotes homogeneity at the ionic level. Importantly, this approach enables the formation of Zn-doped MgTiO_3 crystals at lower calcination temperatures than the solid-state reaction, reducing energy consumption and minimizing side reactions. Despite the advantages noted in previous studies, the literature lacks a comprehensive analysis of the local structural effects of Zn doping within MgTiO_3 , especially at lower synthesis temperatures. This research addresses this gap by achieving highly homogeneous Zn-doped MgTiO_3 nanocrystals with controlled phase composition at reduced temperatures. It provides insights into the structural properties that enhance its potential for nanoscale purity and uniformity applications.

This study hypothesizes that the production of Zn-doped MgTiO_3 using an acidic medium for dissolving metal components enables the synthesis of highly pure nanocrystalline oxide materials at lower calcination temperatures. The objective is to evaluate the effects of calcination temperature and Zn doping on the structural and morphological properties of MgTiO_3 . To prove this hypothesis, we employed advanced characterization

techniques, including XRD, SEM, FTIR, and XAS, to analyze the phase composition, particle morphology, crystallite size, and local atomic environment of the synthesized materials.

■ EXPERIMENTAL SECTION

Materials

Samples were prepared using the dissolved metals mixing method [13-14]. High-purity reagent powders of magnesium (Mg, 99.9%), zinc (Zn, 99.9%), and titanium (Ti, 99.8%) were obtained from Sigma-Aldrich. 37% hydrochloric acid (HCl) solvent was prepared from Merck.

Instrumentation

Characterization using a Bruker D8 Advance XRD was carried out to identify the material's crystal structure and phase composition. This measurement was carried out at the angle of $2\theta = 10\text{--}70^\circ$ with the Cu-K α target ($\lambda_1 = 1.54060 \text{ \AA}$; $\lambda_2 = 1.54443 \text{ \AA}$). Qualitative analysis was carried out using *Match!* software to identify the phase. Meanwhile, quantitative analysis was performed using Rietica software and the Rietveld method to determine the phase composition and lattice parameters. *MAUD ver. 2.999* software was used to estimate the crystallite size. Corrections were involved to consider instrumental peak broadening in the evaluation of phase composition, lattice parameters and crystallite size using both software [15]. The microstructure of the powders was examined using a Phenom Pro-x SEM at 15 kV. FTIR data were collected for the 500 to 4000 cm^{-1} wavenumbers using a Bruker Vertex7.0v FTIR spectrometer to characterize the interatomic bonding states through the vibration spectra. XAS measurements at Ti K-edge were carried out using Beam Line 2.2 at SLRI, Thailand. In order to analyze the phase evolution of the 400 °C-precalcined samples, *in situ* measurements were performed in air by raising the temperature by 10 °C/min up to 700 °C. The temperature was kept constant for 1 s during the XAS measurement.

Procedure

Each metal was dissolved independently in a HCl solution of 12 M concentration. The dissolution was conducted at room temperature for Mg and Zn, while Ti

was dissolved at 65 °C to ensure complete solubilization. The required amounts of Mg, Zn, and Ti chlorides were mixed in the solution according to the doping composition (x) and stirred at room temperature for 5 h. The mixed solution was dried at 110 °C and pre-calcined at 400 °C for 1 h in air. The powder was then calcined at temperatures between 600 and 800 °C for 4 h in air with a heating rate of 10 °C/min. The chemical composition of the samples was set according to the stoichiometry of $\text{Mg}_{1-x}\text{Zn}_x\text{TiO}_3$, where x represents the Zn composition. In this study, we used variations of $x = 0.00, 0.25, 0.50, 0.75,$ and 1.00 to investigate the effects of different Zn concentrations on the properties of the synthesized material.

■ RESULTS AND DISCUSSION

Fig. 1 and 2 show the XRD patterns of the samples with varied calcination temperature and Zn composition. Based on qualitative analysis of the XRD data, the identified phases in the calcined powders were geikielite (MgTiO_3 , COD No. 9011261, lattice system of trigonal, and space group of $R\text{-}3H$), rutile (TiO_2 , COD No. 1011193, lattice system of tetragonal, and space group of $P4_2/mnm$), periclase (MgO , COD No. 9004141, lattice system of cubic, and space group of $Fm\text{-}3m$), and wurtzite (ZnO , COD 1011258, lattice system of hexagonal, and space group of $P6_3mc$).

The Rietveld-based qualitative analysis of XRD data, as mentioned before, begins by noting that the diffraction peaks associated with the presence of geikielite were observed in all the powder samples that underwent calcination at 600 °C. This observation suggests that the geikielite phase was successfully formed at this temperature in our samples. Zhou et al. [16] reported that they were able to obtain the geikielite phase at a relatively high temperature of 850 °C using a solid-state reaction method. In comparison, Liou and Yang [17] reported obtaining geikielite at an even higher temperature of 1100 °C. The key observation in our work is that the dissolved metal mixing method promoted the formation of geikielite at a significantly lower calcination temperature, namely 600 °C. This is a substantial reduction in temperature compared to the

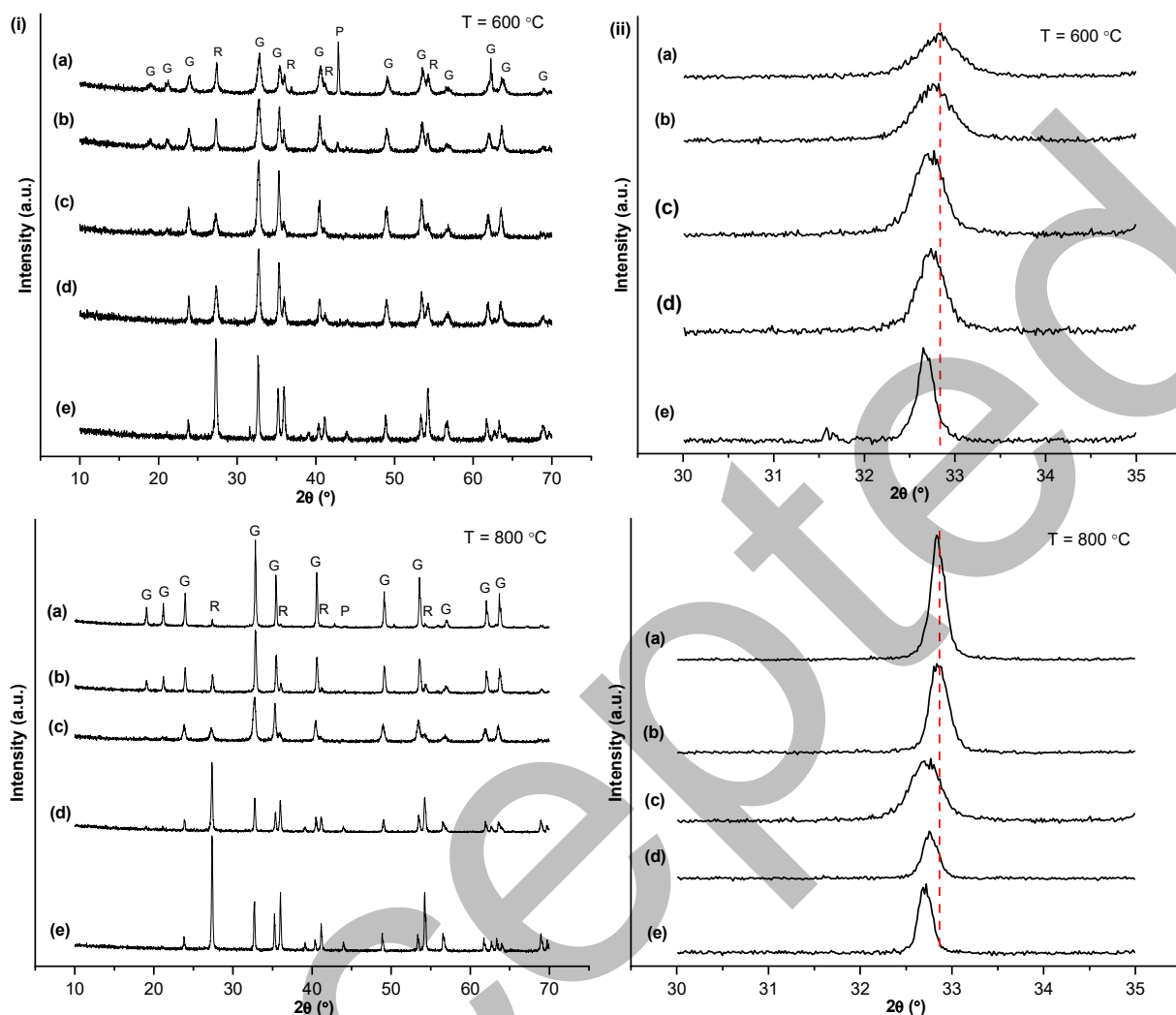


Fig 1. (i) XRD patterns of the powders calcined at 600 and 800 °C with varied dopant Zn composition: (a) 0.00, (b) 0.25, (c) 0.50, (d) 0.75, (e) 1.00, (ii) XRD peak broadening details at $2\theta = 30\text{--}35^\circ$. Symbol: G = geikielite, R = rutile, P = periclase

previous methods mentioned (850 °C and 1100 °C). This passage explains why the dissolved metal mixing method can achieve geikielite formation at lower temperatures. It implies that the observed success can be ascribed to the homogeneity of precursor mixing, particularly in relation to the dissolved metal components.

In summary, the passage highlights that the dissolved metal mixing method was successful in promoting the formation of geikielite at a lower calcination temperature (600 °C) compared to previous methods (850 °C and 1100 °C). This success is attributed to the homogeneity of precursor mixing at the ionic level, which enhances the efficiency of chemical reactions and phase transitions. This finding is significant because it offers a more energy-

efficient and lower-temperature route to obtain geikielite, which can have important implications for materials synthesis and related applications.

A detailed inspection of the XRD peaks found the shift in the position of the geikielite peaks, as shown in Fig. 1 and 2(b). This shift indicates that there have been changes in the crystal lattice parameters of the geikielite phase in response to the introduction of Zn atoms. The diffraction peak shifted to the smaller 2θ angle with the increase of the Zn composition, which can be ascribed to the difference in ionic radii of Zn^{2+} (0.74 Å) and Mg^{2+} (0.72 Å) [7]. In this case, Zn^{2+} ions are slightly larger (have a larger ionic radius) than Mg^{2+} ions. When Zn^{2+} ions are introduced into the crystal lattice of geikielite,

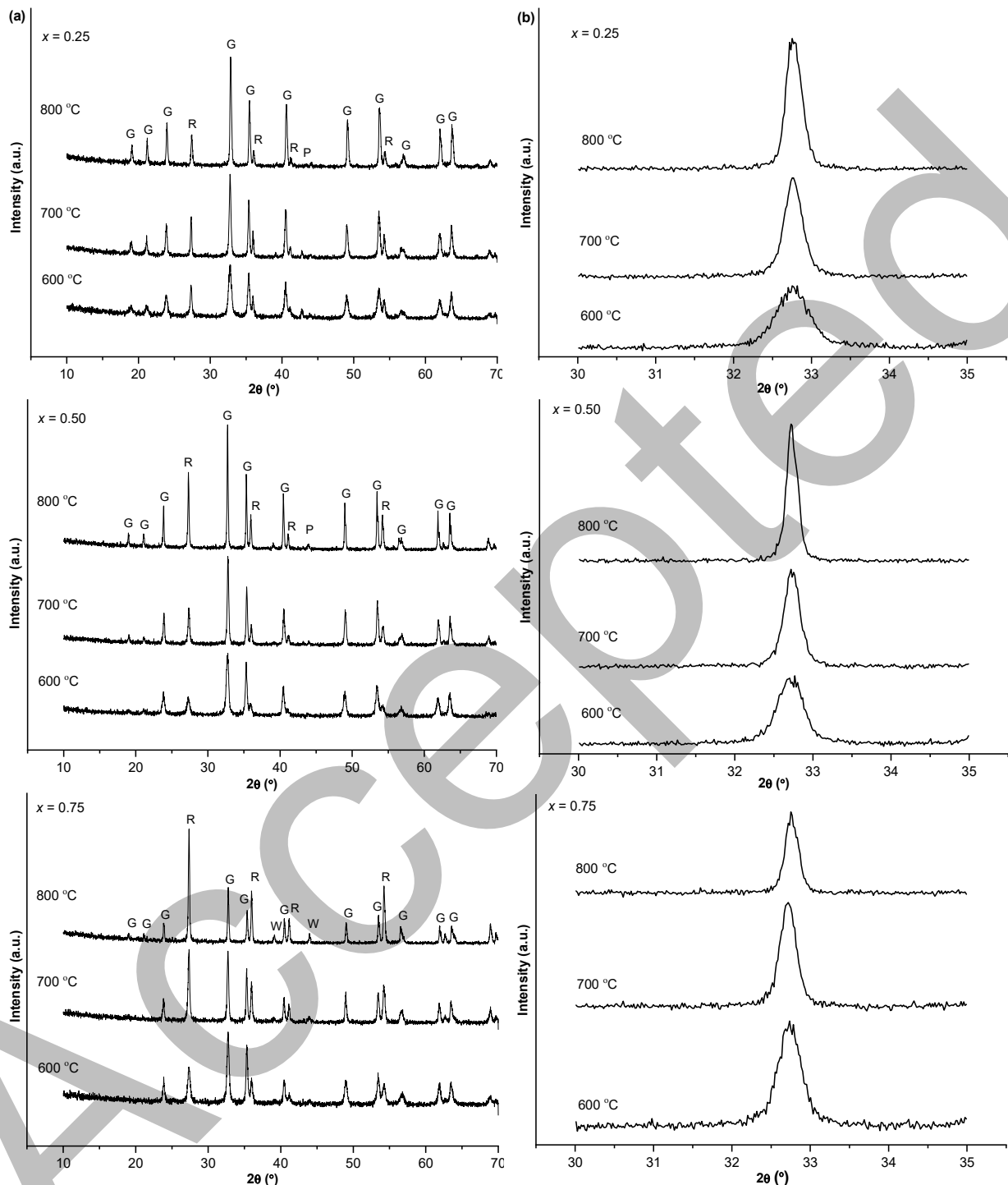


Fig 2. (a) XRD patterns of the calcined powders with varied dopant Zn composition; (b) XRD peak broadening details at $2\theta = 30\text{--}35^\circ$. Symbol: G = geikielite, R = rutile, P = periclase

they occupy positions originally designed for smaller Mg^{2+} ions. The larger ionic radius of Zn^{2+} causes a distortion or expansion of the crystal lattice. This distortion results in a shift in the XRD peak positions to

smaller 2θ angles. Smaller 2θ angles correspond to larger d -spacings between crystal planes. In other words, the crystal lattice becomes more spaced out or expanded due to the larger Zn^{2+} ions. This phenomenon is a crucial

aspect of understanding how introducing dopant ions can affect the crystal structure and properties of materials.

The Rietveld method is a widely used technique in XRD analysis to quantitatively determine the phase composition and structural parameters (such as lattice parameters) of crystalline materials. It involves fitting experimental XRD data with calculated diffraction patterns for different crystal structures and refining the parameters until a good match is achieved. The Rietveld method was applied to the XRD data collected from the samples under investigation. This analysis revealed both the phase composition and lattice parameters of the samples. Phase composition refers to identifying the different crystalline phases present in the material, while lattice parameters describe the dimensions and symmetry of the crystal lattice. The Rietveld calculation was performed using the diffraction data from the International Center for Diffraction Data (ICDD) database to identify the phases and refine the lattice parameters. The results of the quantitative analysis of the

XRD data are presented in Tables 1 and 2. These tables provide information about the identified phases and their corresponding lattice parameters for each sample in the study. Fig. 3 illustrates an example of a refined XRD pattern using Rietica software. This pattern would show the experimental XRD data overlaid with the calculated pattern resulting from the refinement process. The match between the two patterns indicates the quality of the refinement. The acceptance of the refinement using Rietica software was determined by a parameter known as the Goodness-of-Fit (*GoF*), which was required to be less than 4% [18]. The *GoF* is a measure of how well the calculated pattern fits the experimental data. A low *GoF* indicates a good fit, suggesting that the refined parameters accurately describe the material's crystal structure. The quantitative analysis of the XRD data for all calcined powders allowed the determination of the relative weight fraction of various crystalline phases. This means that the technique can estimate the proportion of each identified

Table 1. Rietveld-derived phase composition, volume cell, and crystallite size of the calcined powders (referred to Fig. 1) using Rietica and MAUD softwares. Numbers in parentheses represent estimated standard deviation to associated average value at its least significant level

Sample	Calcination temperature (°C)	Phase composition (wt%)				Geikielite volume cell (Å ³)	Rietica <i>GoF</i>	Geikielite crystallite size (nm)	MAUD <i>GoF</i>
		Geikielite	Rutile	Periclase	Wurtzite				
<i>x</i> = 0	600	69.70 (2)	15.80 (1)	14.50 (3)	0.00	295.08 (6)	1.70	18.00 (1)	1.30
	800	94.30 (1)	2.00 (1)	3.70 (1)	0.00	295.27 (2)	2.10	189.00 (1)	1.50
<i>x</i> = 1	600	48.40 (8)	51.10 (2)	0.00	0.50 (1)	295.61 (5)	1.60	168.00 (3)	2.80
	800	47.30 (4)	52.70 (1)	0.00	0.00	296.11 (3)	1.50	174.00 (1)	3.40

Table 2. Rietveld-derived phase composition, volume cell, and crystallite size of the calcined powders (referred to Fig. 2) using Rietica and MAUD softwares. Numbers in parentheses represent estimated standard deviation to associated average value at its least significant level

Dopant Zn composition (<i>x</i>)	Sample Calcination temperature (°C)	Phase composition (wt%)				Geikielite volume cell (Å ³)	Rietica <i>GoF</i>	Geikielite crystallite size (nm)	MAUD <i>GoF</i>
		Geikielite	Rutile	Periclas	Wurtzite				
0.25	600	81.50 (7)	15.6 (1)	2.90 (8)	0	295.22 (1)	1.80	25.00 (1)	1.30
	700	87.40 (9)	11.5 (3)	1.10 (4)	0	295.34 (5)	2.20	67.00 (5)	1.70
	800	89.00 (8)	9.3 (2)	1.70 (2)	0	295.35 (4)	2.00	85.00 (4)	1.30
0.50	600	86.90 (9)	12.6 (4)	0.50 (2)	0	295.35 (7)	1.70	26.00 (1)	1.30
	700	75.50 (7)	20.7 (4)	3.80 (6)	0	295.57 (4)	1.70	80.00 (4)	2.10
	800	73.40 (7)	22.6 (3)	4.00 (1)	0	295.69 (2)	2.50	118.00 (1)	1.80
0.75	600	76.40 (8)	23.6 (3)	0.00	0	295.45 (6)	2.10	168.00 (1)	1.50
	700	48.80 (4)	51.2 (2)	0.00	0	295.45 (5)	1.70	173.00 (1)	1.90
	800	44.70 (1)	55.3 (1)	0.00	0	295.52 (3)	2.20	179.00 (4)	1.60

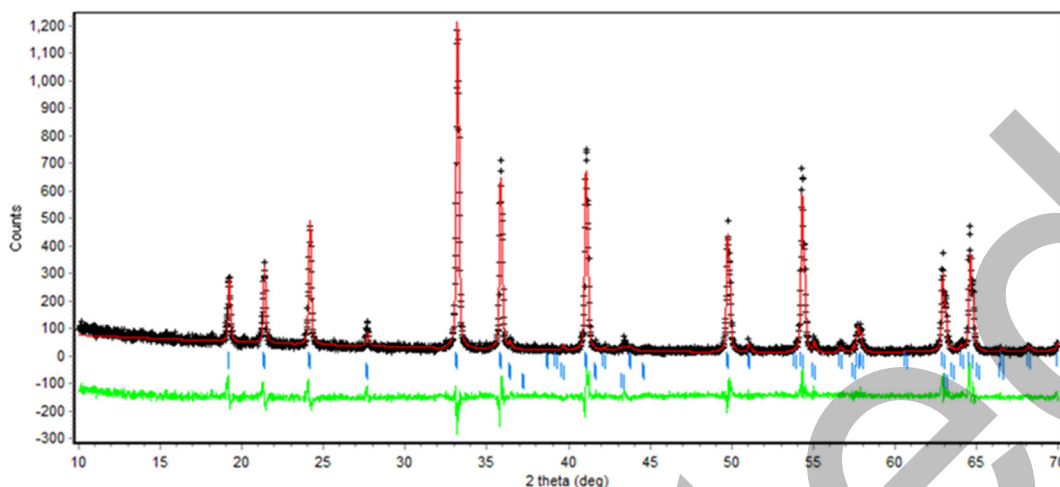


Fig 3. Rietveld refining plot for XRD data of $x = 0.50$ powder calcined at $600\text{ }^{\circ}\text{C}$ using Rietica software with a GoF (Goodness-of-Fit) value of 1.7. Note: red curve: calculated diffraction pattern, black cross: measured diffraction data, green curve: residual, and blue bar: peak positions

phase in the sample. The effects of calcination temperature and the composition of Zn on the phase composition and lattice parameters are summarized in Fig. 4. The figure presents how these factors influence the relative abundance of different phases and the lattice parameters of the materials.

For the $x = 0$ sample, the composition of geikielite increased with raising the calcination temperature from 600 to $800\text{ }^{\circ}\text{C}$. A similar trend can be seen in the $x = 0.25$ sample. However, an interesting trend was observed for the sample with $x = 0.50$ (a higher Zn composition). As

the calcination temperature increased, the composition of geikielite decreased. This implies that at higher temperatures, less geikielite was formed in this sample. It suggests that this is due to the decomposition of geikielite into two other compounds: rutile (TiO_2) and periclase (MgO , in the amorphous phase) [19]. In other words, at higher temperatures, geikielite in this sample broke down into these two materials. The decomposition of the compound $\text{Zn}_{1-x}\text{Mg}_x\text{TiO}_3$ starts at a specific temperature. According to Jaramillo-Fierro et al. [19], this decomposition process begins at $700\text{ }^{\circ}\text{C}$. This means that

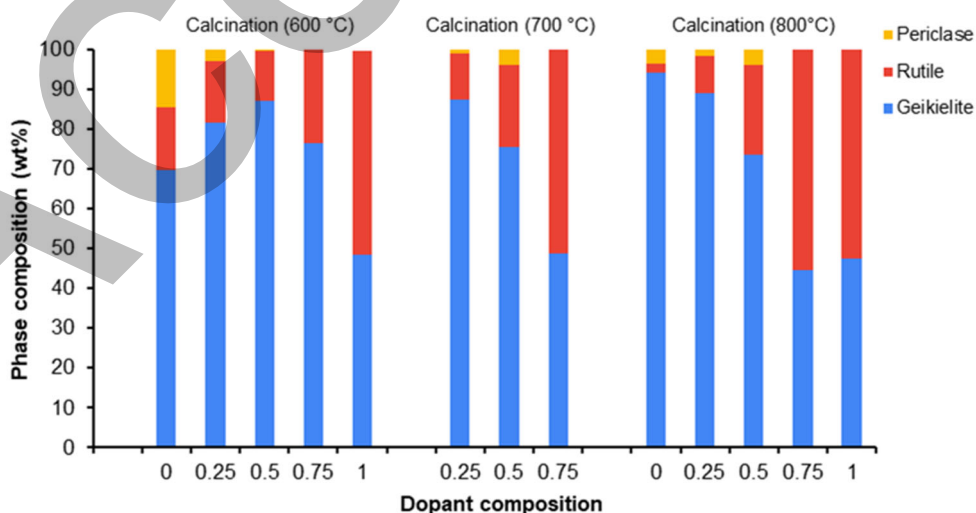


Fig 4. Phase compositions by the Rietveld analysis with the Rietica software for samples with different calcination temperatures and Zn compositions

when the calcination temperature reaches or exceeds 700 °C, the geikielite in the $x=0.50$ sample starts to transform into rutile and periclase. This observation underscores the importance of both composition and temperature control when synthesizing materials with specific properties.

The cell volume of a crystalline material refers to the amount of space occupied by the atoms or ions within its crystal structure. It's an important structural property that can change based on the composition of the material. Fig. 5 shows how the cell volume of geikielite changes with varying levels of Zn composition x . It is noted previously that the cell volume increased linearly with the increase in x , as expected from the peak shift observed in Fig. 1(b) and 2(b). In other words, as we add more Zn to the geikielite structure (increasing x), the cell volume of the resulting material also increases. This suggests that the presence of Zn atoms directly impacts the arrangement of atoms within the geikielite crystal lattice. Moreover, it highlights a crucial observation that the cell volume of geikielite increased up to $x = 1$. This implies that the solubility limit of Zn in the geikielite structure is close to $x = 1$ for samples calcined at 600 °C. In other words, geikielite can

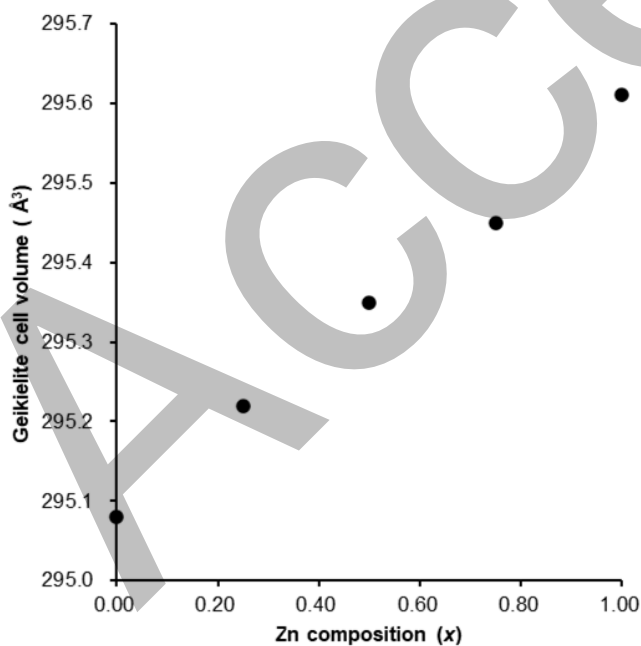


Fig 5. Cell volume of the geikielite phase as a function of Zn composition by the Rietveld analysis with the *Rietica* software for samples calcined at 600 °C

accommodate a significant amount of Zn within its crystal lattice, and this accommodation increases with increasing Zn composition up to $x = 1$. Except for the sample with $x = 1$ calcined at 600 °C, the crystalline phase of ZnO was not identified in the samples. This means that in most samples, the primary crystalline phase remained geikielite, and the presence of ZnO was minimal or negligible. Even in the $x = 1$ sample calcined at 600 °C, where some ZnO was identified, its composition was stated to be as low as 0.5 wt.%. This indicates that even when the solubility limit of Zn in geikielite is relatively high, the amount of ZnO formed is still limited. This passage concludes that the low composition of ZnO in the $x = 1$ sample is consistent with the high solubility of Zn in geikielite. In other words, geikielite can accommodate a significant amount of Zn within its crystal lattice without forming a separate ZnO phase. This information is crucial for understanding the structural properties of the material and its potential applications.

The crystallite size refers to the size of individual crystalline grains within a material. It is a fundamental property that reflects the size of the structural units making up a crystalline substance. In this study, the crystallite size of geikielite is evaluated using XRD patterns, and the analysis is performed using the Rietveld-based *MAUD* software. This software allows for the determination of crystallite size based on XRD data. It's worth noting that instrument line broadening correction was applied during the analysis. This correction helps remove the effects of the X-ray equipment itself on the observed peak widths [20]. For the $x = 0.00$ and $x = 0.25$ samples, it is observed that the crystallite size increases with the calcination temperature. This trend is expected because, in general, crystalline grains tend to grow larger as the temperature of the material increases. This is a common behavior in materials science. However, for the samples with higher Zn composition ($x = 0.75$ and $x = 1.00$), the growth of crystallite size is not as evident, especially when calcined at higher temperatures. This is because the crystallite size was already relatively large (168 nm) when calcined at 600 °C. As described earlier in the text, the partial

decomposition of the geikielite phase may play a role in the observed size changes when the Zn composition exceeds $x = 0.75$. This implies that some of the geikielite may be breaking down into other phases at higher Zn compositions ($x = 0.75$ and $x = 1.00$) and higher calcination temperatures. Decomposition can affect the overall crystallite size and its growth behavior. As determined by XRD analysis, the crystallite size is approximately an order of magnitude smaller than the particle size observed in the SEM images shown in the next passage. This highlights a distinction between the size of individual crystalline grains (crystallite size) and the overall size of the particles, which can be composed of multiple crystallites.

Fig. 6 presents SEM images of sample powders after undergoing a calcination. The images reveal the morphology (shape and size) of the particles in the samples. Here's a detailed breakdown of the information provided. Fig. 6 depicts the appearance of the sample

powders after the calcination process. Calcination involves heating a material to high temperatures to remove volatile substances, induce chemical reactions, or alter its physical and chemical properties. As observed in the SEM image, the samples consist of particles approximately $1\ \mu\text{m}$ in diameter. This means that the majority of particles in the sample have a very similar size and shape, appearing as small spheres. While the individual particles are approximately $1\ \mu\text{m}$ in diameter, it's noted that smaller particles tend to agglomerate. In other words, some of the smaller particles cluster together to form larger structures within the sample. This agglomeration can be seen in the SEM images. Fig. 6(a) and (b) compare particle morphology of $800\ \text{°C}$ -calcined samples with $x = 1.00$ and 0.75 . Fig. 6(b–d) show the variation of the morphology for the $x = 0.75$ sample with calcination temperature between 600 and $800\ \text{°C}$. Little change in the particle size is apparent with x and the calcination temperature.

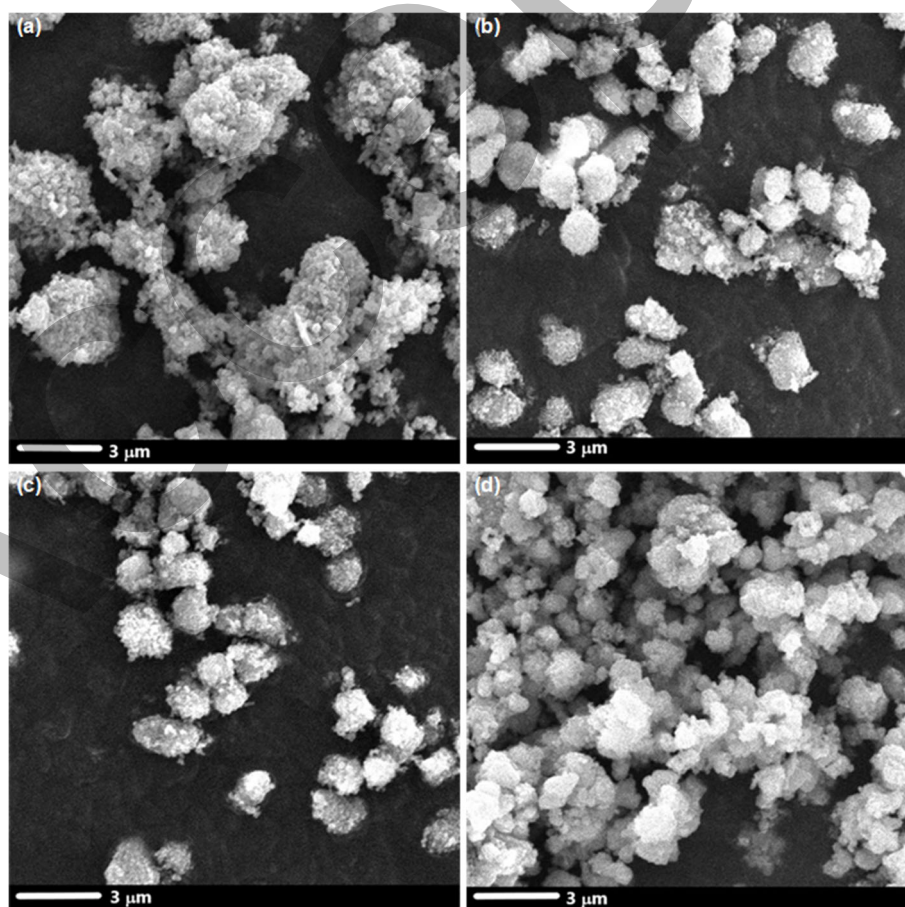


Fig 6. SEM image of calcined powders (a) $x = 1$, $800\ \text{°C}$, (b) $x = 0.75$, $600\ \text{°C}$, (c) $x = 0.75$, $700\ \text{°C}$, and (d) $x = 0.75$, $800\ \text{°C}$

FTIR characterization was carried out to identify functional groups in Zn-doped MgTiO_3 powder samples. FTIR spectroscopy is a technique used to identify the functional groups and chemical bonds present in a material by analyzing the absorption of infrared light at specific wavenumbers. The results of the FTIR test were analyzed by examining the specific peaks in the FTIR spectra. These peaks are associated with vibrational modes of atoms and molecules, and their positions on the spectrum are measured in wavenumbers. The FTIR spectra of the samples are presented in Fig. 7 and 8. In these spectra, three absorption peaks are identified, labeled as peaks A,

B, and C. At peak A, a wide absorption band appears at a wavenumber of approximately 700 cm^{-1} . This band indicates a typical Ti–O vibration [21]. Peak B appears as a sharper peak in the FTIR spectrum and is located in the range of wavenumbers between 530 and 540 cm^{-1} . This peak is associated with the O–Ti–O vibrational band, suggesting the presence of oxygen bridges between Ti atoms [21]. Peak C is another sharp peak at wavenumbers between 440 and 446 cm^{-1} . It is associated with a vibrational band involving Mg–O or Zn–O bonds [21]. The presence of these three vibrational bands (O–Ti–O, Mg–O, or Zn–O) is consistent with the formation of solid

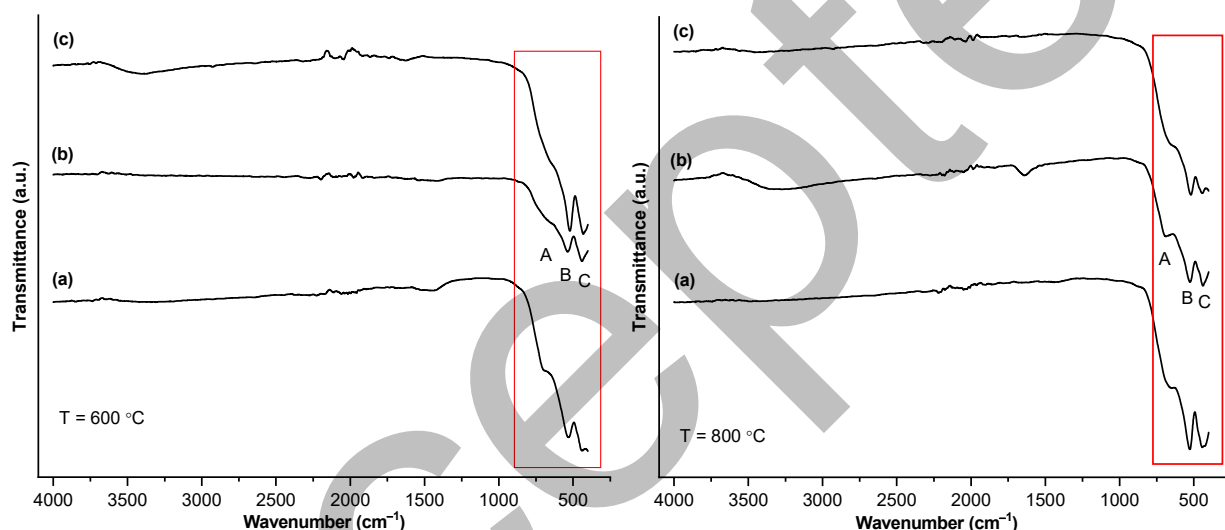


Fig 7. FTIR spectra of sample powders calcined at 600 and 800 °C with varied dopant composition: (a) $x = 0.00$, (b) $x = 0.25$, (c) $x = 0.50$

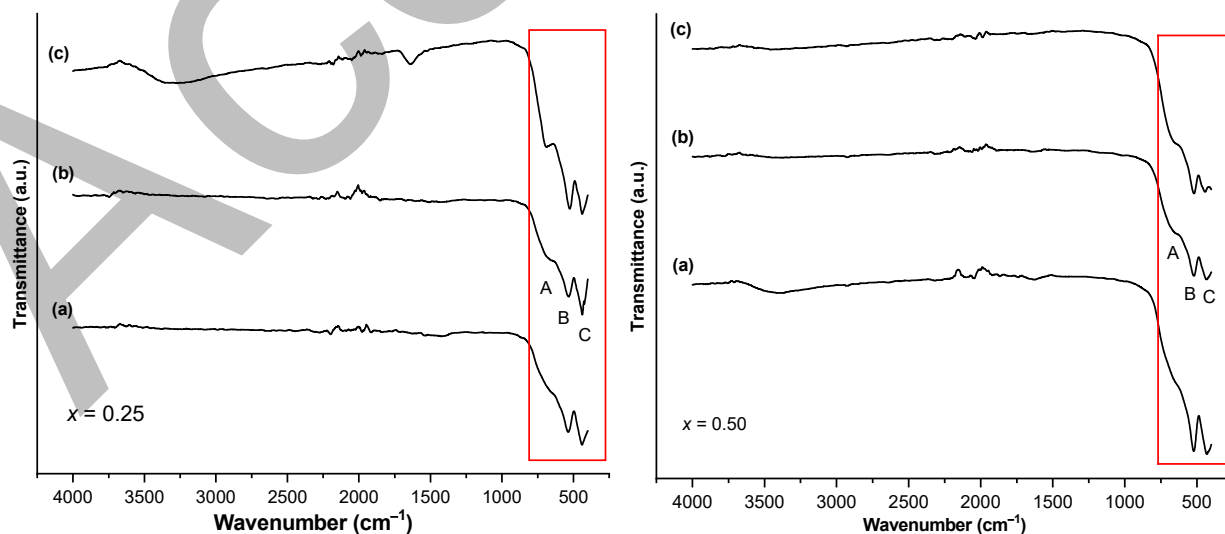


Fig 8. FTIR spectra of sample powders with varied Zn composition calcined at: (a) 600 °C, (b) 700 °C, and (c) 800 °C

solutions of geikielite, as shown by the XRD analysis. This means that the information obtained from FTIR analysis aligns with the results from XRD analysis, which confirmed the presence of geikielite and the incorporation of Zn into the material.

To analyze the phase evolution of the sample, *in situ* XAS measurements were made on a 400 °C pre-calcined powder sample by raising the temperature by 10 °C/min up to 700 °C. XANES is a spectroscopy technique used to analyze the absorption of X-rays by a material as a function of X-ray energy near the absorption edge of an element of interest. It provides information about the local environment of that element in the material. After collecting experimental XANES data, it often appears as a complex spectrum with multiple peaks, edges, and features. To extract quantitative information from this data and to better understand the underlying local environment, we fit the spectrum using mathematical functions, such as Gaussian functions. Gaussian functions are bell-shaped curves used to model peaks or features in a spectrum. They are defined by parameters like the center (peak position), width (standard deviation), and intensity (amplitude). The XANES spectrum was fitted (mathematically modeled) using eight Gaussian functions. Each Gaussian function corresponds to a specific peak or feature in the XANES spectrum. The purpose of fitting the XANES spectrum is to deconvolute (separate) the overlapping peaks and features, quantify their positions, widths, and intensities, and extract meaningful information about the local environment of the material. Gaussian functions are commonly used for this purpose because they are mathematically well-behaved and can provide a good approximation to the shapes of spectral peaks. After fitting, the researchers would obtain values for the parameters of each Gaussian function, such as the energy positions of the peaks (center), their widths, and intensities. These parameters can reveal details about the energy levels and bonding environments of the element of interest.

In summary, fitting the XANES spectrum with Gaussian functions is a common analytical technique used to extract quantitative information from complex XANES data. It allows researchers to identify and

characterize the individual peaks and features in the spectrum, providing insights into the local environment of the studied element. Fig. 9 compares the Ti K-edge XANES of undoped MgTiO₃ powder samples ($x = 0$) at different temperatures. Seven peaks, denoted by A to G, were identified in the range of 4950–5090 eV. The XANES spectrum was fitted to the superposition of eight Gaussian functions centered at peaks A–G with an extra peak located at around 5020 eV. A typical fitted result is shown in Fig. 10. Fig 11 compares the Ti K-edge XANES of five Zn-doped MgTiO₃ powder samples ($x = 0.00, 0.25, 0.50, 0.75$ and 1.00) measured at 600 °C. The variation of peak positions with temperatures for five samples are summarized in Table 3.

In XANES spectra of titanates, the spectrum is typically divided into two regions: the pre-edge and main-edge regions. These regions correspond to different energy ranges of the XANES spectrum and reveal different types of information about the Ti atoms in the material. The presence of peaks A and B in the pre-edge region of the Ti K-edge XANES spectrum are specific features that provide insights into the local environment of Ti atoms. Experimental and theoretical approaches are employed to interpret and understand XANES spectra [22]. Theoretical calculations are performed to simulate the XANES spectrum and compare it to experimental data to gain a deeper understanding. In previous studies, density functional theory (DFT)

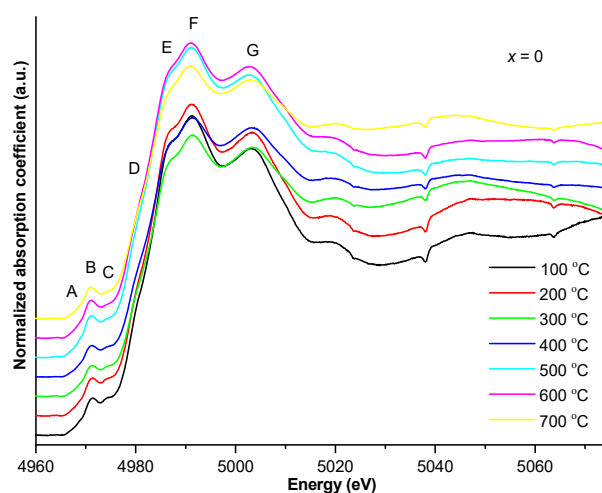


Fig 9. Ti K-edge XANES spectrum of the $x=0$ sample powder measured at 100–700 °C

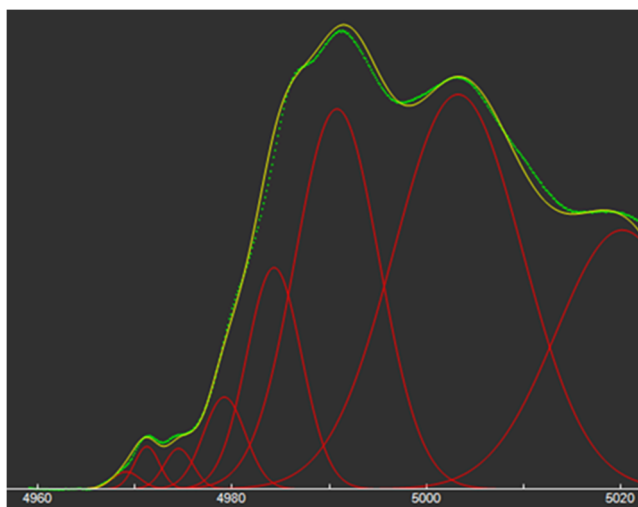


Fig 10. Ti K-edge XANES spectrum of the $x=0$ sample measured at 700 °C (green line) and fitted results (yellow line) using eight Gaussian functions (red lines)

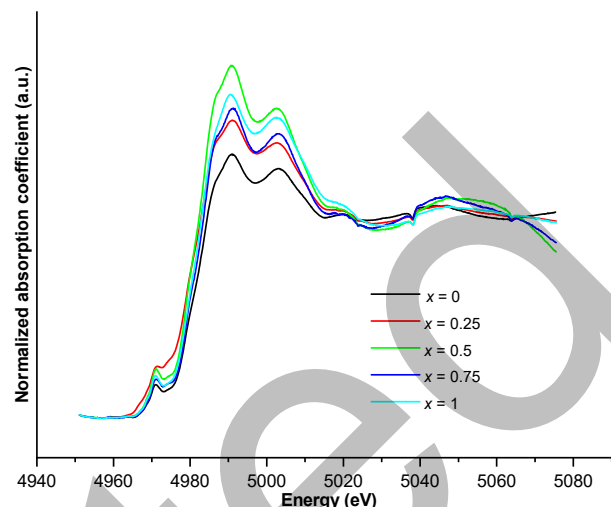


Fig 11. Ti K-edge XANES spectrum of the sample powders with different Zn composition measured at 600 °C

Table 3. Peak positions in Ti K-edge XANES spectra of the $x = 0$ sample powder in the range of 4960–5075 eV by *in-situ* measurement at 100–700 °C as a result of peak fittings (referred to Fig. 9). Numbers in parentheses represent the estimated standard deviation to the associated average value at its least significant level

T (°C)	Peaks in Ti K-edge XANES spectra (eV)						
	A	B	C	D	E	F	G
100	4967.43 (1)	4971.12 (4)	4973.98 (1)	4980.21 (1)	4985.69 (2)	4991.75 (1)	5002.70 (2)
200	4967.42 (1)	4971.12 (4)	4974.09 (3)	4980.36 (1)	4985.62 (1)	4991.69 (2)	5002.94 (1)
300	4967.41 (1)	4971.11 (1)	4974.04 (1)	4980.14 (1)	4985.81 (1)	4991.74 (1)	5003.20 (2)
400	4967.43 (2)	4971.10 (2)	4974.06 (3)	4980.33 (2)	4985.67 (1)	4991.66 (1)	5003.18 (2)
500	4967.42 (2)	4970.92 (2)	4974.11 (2)	4979.88 (1)	4985.87 (2)	4991.68 (2)	5002.59 (2)
600	4967.35 (1)	4970.95 (1)	4974.02 (1)	4979.97 (2)	4985.72 (1)	4991.73 (1)	5002.53 (2)
700	4967.32 (1)	4970.95 (1)	4974.15 (1)	4979.91 (1)	4985.76 (2)	4991.75 (2)	5002.95 (1)

Table 4. Peak positions in Ti K-edge XANES spectra of powders with different Zn composition in range of 4960–5075 eV by *in-situ* measurement at 600 °C as a result of peak fittings (referred to Fig. 11). Numbers in parentheses represent the estimated standard deviation to the associated average value at its least significant level

x	Peaks in Ti K-edge XANES spectra (eV)						
	A	B	C	D	E	F	G
0.00	4967.35 (1)	4970.95 (1)	4974.02 (1)	4979.97 (2)	4985.72 (1)	4991.73 (1)	5002.53 (2)
0.25	4967.51 (2)	4971.03 (1)	4973.94 (2)	4980.18 (1)	4985.23 (4)	4991.50 (3)	5002.47 (2)
0.50	4967.51 (1)	4970.99 (4)	4974.41 (3)	4980.05 (6)	4985.13 (5)	4991.40 (4)	5002.41 (1)
0.75	4968.20 (1)	4970.78 (5)	4974.43 (3)	4980.30 (5)	4984.91 (3)	4990.93 (3)	5004.18 (1)
1.00	4968.38 (2)	4970.87 (7)	4974.06 (1)	4980.36 (3)	4984.95 (1)	4991.66 (2)	5003.02 (1)

calculations, which involve solving the Schrödinger equation with approximations to model the electronic structure of materials, have been widely used to simulate the XANES spectra of titanates. These calculations

consider the interactions of X-rays with the material's electronic states and include the concept of a Ti-1s core hole [23]. While DFT calculations were not employed in this study, we refer to these theoretical approaches to

enrich the discussion of the XANES spectra. DFT has effectively reproduces the features observed in the main edge region of the XANES spectrum, which is related to electric dipole transitions. In XANES spectroscopy, the absorption of X-rays is described as an electric dipole transition where electrons in core levels are excited to higher energy levels. Another theoretical approach, Green's function formulation of multiple scattering theory, has successfully reproduces the features in the main edge of the XANES spectrum. This approach considers the interactions of X-rays with multiple atoms in the material. One must also consider electric quadrupole transitions to accurately reproduce the features in the pre-edge region (where peaks A and B are located) [24]. These transitions involve changes in the spatial distribution of electron charge density around the Ti atom and provide information about the local symmetry and coordination environment [23].

Ti K-edge XANES spectroscopy is a sensitive technique that provides information about the electronic states of Ti. It specifically probes the electronic transitions involving Ti-4*p* electrons for electric dipole transitions and Ti-3*d* electrons for electric quadrupole transitions. Ti K-edge XANES can be applied to a wide range of materials, including bulk crystals (well-ordered structures), defective crystals (crystals with structural imperfections or defects), nano-sized crystals (very small crystals), and amorphous materials (materials lacking long-range order in atomic arrangement). This versatility makes it a valuable tool for studying various types of materials. As a result, it is highly sensitive to the local coordination environment of Ti atoms within a material. Experimental finds that the peak positions in the Ti K-edge XANES spectra of titanates can shift by approximately ± 2 eV depending on the local coordination environment of Ti atoms [25]. This shift is significant because it reflects changes in the environment of the Ti atoms due to variations in their local surroundings. It is also highlighted that computed results obtained through the multiple scattering theory showed similar shifts in peak positions. This indicates that theoretical calculations are in agreement with experimental observations, validating the use of theoretical models to interpret Ti K-edge XANES data [24].

In XANES spectroscopy, the position of peaks in the spectrum corresponds to specific energy levels associated with the electronic transitions of the element being studied. In this case, the focus is on Ti and its local atomic environment. The study involves subjecting the samples to a heating process, ranging from 100 to 700 °C. This heating measurement is used to investigate how the XANES peak positions change as the temperature increases, which can provide insights into any alterations in the local atomic environment of Ti atoms. According to the data presented in Tables 3 and 4, for the sample with $x = 0$ (no Zn doping), the peak positions in the XANES spectra did not shift significantly during the heating process from 100 to 700 °C. This lack of significant peak position shift indicates that the local atomic environment of Ti remained relatively stable and did not undergo remarkable changes as the temperature increased. At 600 °C, the dependence of peak positions on the Zn composition was small. In other words, when comparing samples with different levels of Zn doping (from $x = 0$ to higher values), the peak positions did not show substantial shifts at 600 °C. This implies that the presence of Zn in the samples did not significantly alter the local atomic environment of Ti at this temperature. The lack of significant peak position shifts during the heating process and the small dependence on Zn composition suggest that both the undoped ($x = 0$) and the Zn-doped samples exhibited relative stability in the local atomic environment of Ti. This stability is observed even as the temperature increases and with the addition of Zn atoms, indicating that the Ti coordination environment was not notably disrupted or transformed under these conditions. In summary, these observations provide insights into the stability of the Ti coordination environment under different conditions.

The synthesis route of Zn-doped MgTiO₃ ($x = 0.2$) via the dissolved metals mixing method has been studied by Ermawati et al. [14] using TG/DTA, XRD and FTIR. In their work, the dried powder before the calcination was composed of MgCl₂·6H₂O, rutile (TiO₂), and ZnCl₂ with amorphous Ti compounds. In the range of 220–380 °C, the transition of Mg_{1-x}Zn_xCl₂·H₂O to Mg_{1-x}Zn_x(OH)Cl occurred. Then, the formation of the solid

solution, $Mg_{1-x}Zn_xTiO_3$, was initiated at temperatures as low as 400 °C, as a result of the reaction of $Mg_{1-x}Zn_x(OH)Cl$ and TiO_2 . In contrast, in our study, the Ti K-edge XANES of the 400 °C-pre calcined sample (Fig. 9) found little change in the peak positions and spectral shapes during heating from 100 to 700 °C. This implies that the geikielite formation was almost completed in the 400 °C-pre calcined sample, which is consistent with the results by Ermawati et al. [14]. However, the novelty of our study lies in the detailed analysis of the temperature-dependent structural evolution, including how the varying Zn composition influences the formation of $Mg_{1-x}Zn_xTiO_3$, as well as the precise characterization of the phase transitions through multiple techniques. Our findings provide new insights into the thermal behavior of the material and its phase formation dynamics, expanding upon the work of Ermawati et al. [14] by offering a deeper understanding of how calcination temperature and Zn doping affect the formation and stability of the geikielite phase.

■ CONCLUSION

The paper presented here evaluated the role of calcination temperature and Zn dopant composition on phase composition and the evolution of the local atomic environment of Zn-doped $MgTiO_3$ powders. A simple method of mixing dissolved metals has been adopted. Geikielite composition reaches 94.3 wt.% for an undoped powder ($x = 0$) calcined at 800 °C. Successful synthesis of the Zn-doped $MgTiO_3$ nanocrystals at temperatures much lower than that required by the solid-state reaction method was well demonstrated. The increase in the calcination temperature and Zn composition indicates a change in the crystallite size and lattice parameters, respectively. The particles have a spherical morphology ($\sim 1 \mu m$) and some agglomeration occurs. The local atomic environment of Ti in geikielite did not change remarkably during heating or with the doping of Zn.

■ ACKNOWLEDGMENTS

This research was supported by the Institute for Research and Community Services (LPPM) ITK and the Indonesian Toray Science Foundation (ITSF) through Science and Technology Research Grant.

■ CONFLICT OF INTEREST

The authors have no relevant financial or non-financial interests to disclose.

■ AUTHOR CONTRIBUTIONS

Conceptualization, methodology, and validation: Musyarofah, Lusi Ernawati, and Budi Prayitno; resources and investigation: Zakiah Mohamed, Yingyot Poo-arporn, and Gatut Yudoyono; review and supervision: Isao Tanaka. All authors agreed to the published version of the manuscript.

■ REFERENCES

- [1] Magar, H.S., Mansour, A.M., and Hammad, A.B.A., 2024, Advancing energy storage and supercapacitor applications through the development of Li^+ -doped $MgTiO_3$ perovskite nano-ceramics, *Sci. Rep.*, 14 (1), 1849.
- [2] Mallick, P., Mishra, S., Fatma, N., Das, D.K., Moharana, S., and Satpathy, S.K., 2024, "Microwave Dielectric Properties of Electroceramics" in *Defects Engineering in Electroceramics for Energy Applications*, Eds. Kumar, U., Springer Nature Singapore, Singapore, 351–370.
- [3] Rabha, S., and Dobbidi, P., 2021, Structural, electrical properties and stability in microwave dielectric properties of $(1-x)MgTiO_{3-x}SrTiO_3$ composite ceramics, *J. Alloys Compd.*, 872, 159726.
- [4] Mohapatra, S., Barman, R., Das, T.K., Badapanda, T., Huang, Y., Xiao, J., and Tripathy, S.N., 2024, Structure property correlation of $(1-x)MgTiO_3 - xSrTiO_3$ microwave dielectric ceramics for dielectric resonator antenna applications, *Ceram. Int.*, 50 (18, Part A), 31792–31808.
- [5] Bouzaid, A., Ziat, Y., Belkhanchi, H., Hamdani, H., Koufi, A., Miri, M., Laghlimi, C., and Zarhri, Z., 2024, Ab initio study of the structural, electronic, and optical properties of $MgTiO_3$ perovskite materials doped with N and P, *E3S Web Conf.*, 582, 02006.
- [6] Musyarofah, M., Damanik, E.F., Husain, H., Yudoyono, G., Mohamed, Z., Poo-arporn, Y., and Prayitno, B., 2022, Local structure studies of magnesium titanate powders using time-resolved

- X-ray absorption spectroscopy (TRXAS) measurements, *AIP Conf. Proc.*, 2708 (1), 060001.
- [7] Musyarofah, M., Damanik, E.F., Septiana, A.R., Shoodiqin, D.M., Husain, H., and Yudoyono, G., 2022, Phase study of $Mg_{1-x}Zn_xTiO_3$ powders prepared by dissolved metals mixing method, *AIP Conf. Proc.*, 2652 (1), 050013.
- [8] Feng, Y., Wu, J., Chi, Q., Li, W., Yu, Y., and Fei, W., 2020, Defects and aliovalent doping engineering in electroceramics, *Chem. Rev.*, 120 (3), 1710–1787.
- [9] Grünert, W., and Klementiev, K., 2020, X-ray absorption spectroscopy principles and practical use in materials analysis, *Phys. Sci. Rev.*, 5 (4), 2017018.
- [10] Bin Adnan, M.A., Arifin, K., Minggu, L.J., and Kassim, M.B., 2018, Titanate-based perovskites for photochemical and photoelectrochemical water splitting applications: A review, *Int. J. Hydrogen Energy*, 43 (52), 23209–23220.
- [11] Shariatnia, Z., and Karimzadeh, Z., 2024, Perovskite oxides as efficient bioactive inorganic materials in tissue engineering: A review, *Mater. Today Chem.*, 35, 101846.
- [12] Musyarofah, M., Soontaranon, S., Limphirat, W., Triwikantoro, and Pratapa, S., 2019, XRD, WAXS, FTIR, and XANES studies of silica zirconia systems, *Ceram. Int.*, 45 (12), 15660–15670.
- [13] Pratapa, S., Baqiya, M.A., Istianah, I., Lestari, R., and Angela, R., 2014, A simple dissolved metals mixing method to produce high-purity $MgTiO_3$ nanocrystals, *AIP Conf. Proc.*, 1586 (1), 39–42.
- [14] Ermawati, F.U., Suasmoro, S., and Suminar, P., 2015, A simple dissolved metals mixing route to prepare nanostructured $Mg_{0.8}Zn_{0.2}TiO_3$ solid solution, *Adv. Mater. Res.*, 1112, 47–52
- [15] Musyarofah, M., Sari, Y.P., Hilmi, A.R., Asrori, M.Z., Triwikantoro, T., Zainuri, M., Kim, B.N., and Pratapa, S., 2023, Ultra-dense (Bi, V, B)-oxide-added zircon ceramics fabricated by liquid-phase assisted spark plasma sintering (SPS), *Mater. Res. Express*, 10 (5), 055002.
- [16] Zhou, X., Yuan, Y., Xiang, L., and Huang, Y., 2007, Synthesis of $MgTiO_3$ by solid state reaction and characteristics with addition, *J. Mater. Sci.*, 42 (16), 6628–6632.
- [17] Liou, Y.C., and Yang, S.L., 2007, Calcium-doped $MgTiO_3$ - $MgTi_2O_5$ ceramics prepared using a reaction-sintering process, *Mater. Sci. Eng., B*, 142 (2), 116–120.
- [18] Young, R.A., 1995, *The Rietveld Method*, Oxford University Press, New York, USA.
- [19] Jaramillo-Fierro, X., González, S., Jaramillo, H.A., and Medina, F., 2020, Synthesis of the $ZnTiO_3/TiO_2$ nanocomposite supported in Ecuadorian clays for the adsorption and photocatalytic removal of methylene blue dye, *Nanomaterials*, 10 (9), 1981.
- [20] Hassanzadeh-Tabrizi, S.A., 2023, Precise calculation of crystallite size of nanomaterials: A review, *J. Alloys Compd.*, 968, 171914.
- [21] Cai, Z., Zhou, H., Song, J., Zhao, F., and Li, J., 2011, Preparation and characterization of $Zn_{0.9}Mg_{0.1}TiO_3$ via electrospinning, *Dalton Trans.*, 40 (33), 8335–8339.
- [22] Henderson, G.S., de Groot, F.M.F., and Moulton, B.J.A., 2014, X-ray absorption near-edge structure (XANES) spectroscopy, *Rev. Mineral. Geochem.*, 78 (1), 75–138.
- [23] Yamamoto, T., Mizoguchi, T., and Tanaka, I., 2005, Core-hole effect on dipolar and quadrupolar transitions of $SrTiO_3$ and $BaTiO_3$ at Ti K edge, *Phys. Rev. B*, 71 (24), 245113–245117
- [24] Mathew, K., Zheng, C., Winston, D., Chen, C., Dozier, A., Rehr, J.J., Ong, S.P., and Persson, K.A., 2018, High-throughput computational X-ray absorption spectroscopy, *Sci. Data*, 5 (1), 180151.
- [25] Tobase, T., Yoshiasa, A., Komatsu, T., Maekawa, T., Hongu, H., Okube, M., Arima, H., and Sugiyama, K., 2019, Titanium local coordination environments in Cretaceous–Paleogene and Devonian–Carboniferous boundary sediments as a possible marker for large meteorite impact, *Phys. Chem. Miner.*, 46 (7), 675–685.